

Retrieving transient magnetic fields of ultrarelativistic laser plasma via ejected electron polarization

Zheng Gong,* Karen Z. Hatsagortsyan,† and Christoph H. Keitel
Max-Planck-Institut für Kernphysik, Saupfercheckweg 1, 69117 Heidelberg, Germany
(Dated: March 3, 2022)

Interaction of an ultrastrong short laser pulse with non-prepolarized near-critical density plasma is investigated in an ultrarelativistic regime, with an emphasis on the radiative spin polarization of ejected electrons. Our particle-in-cell simulations show explicit correlations between the angle resolved electron polarization and the structure and properties of the transient quasistatic plasma magnetic field. While the magnitude of the spin signal is the indicator of the magnetic field strength created by the longitudinal electron current, the asymmetry of electron polarization is found to gauge the island-like magnetic distribution which emerges due to the transverse current induced by the laser wave front. Our studies demonstrate that the spin degree of freedom of ejected electrons could potentially serve as an efficient tool to retrieve the features of strong plasma fields.

Magnetic fields play a crucial role in various plasma collective phenomena and nonlinear quantum electrodynamic processes in extreme environments of laboratory and universe [1–3]. The astrophysical magnetic fields can govern the internal structure of interstellar shocks [4], mediate the radio wave emission nearby neutron stars [5], induce baryon inhomogeneities [6], and catalyse the dark matter formation [7]. Self-generated fields with strength $\sim 10^4$ Tesla have been produced in high-intensity plasma experiments [8–12], and the guidance of jet flows by laboratory magnetic fields helps interpret the evolution of young stellar objects [13–15]. With recent advancement of ultrastrong laser techniques [16–22] more extreme conditions and larger fields are expected in ultrarelativistic laser plasma interaction [23–29].

Generally, detection of plasma magnetic fields requires an external probe beam, where the field information is imprinted in the velocity space of charged particles [30–35] or the rotated polarization vector of the optical beam [36–39]. However, these conventional methods are inapplicable for scenarios with unprecedented field strength, ultrashort time scale (\sim fs), and overcritical plasma density [40]. Furthermore, the spin, an intrinsic property of particles, offers a new degree of freedom of information, which is widely utilized in exploring magnetization of solids [41], nucleon structure [42], and phenomena beyond the standard model [43]. In extreme laser fields there is a strong coupling of the electron spin to the laser magnetic field [44–48], which may yield radiative spin polarization (SP) [49–52], i.e., polarization of electrons due to spin-flip during photon emissions. Even though in the oscillating field the electron net SP is suppressed, fast polarization of a lepton beam with laser pulses becomes possible when the symmetry of the monochromatic field is broken, such as in an elliptically polarized, or in two-color laser pulses [53–57]. Because of collective effects, more complex spin dynamics occurs in strong laser field interaction with plasma. Consequently, the question arises if it is possible to employ the spin signal of spontaneously ejected particles from plasma to

retrieve information on transient plasma fields.

In this Letter, based on particle-in-cell (PIC) simulations, we investigate the ultrarelativistic dynamics of a short strong pulse interacting with a non-prepolarized near-critical density plasma, see Fig. 1. Special attention is devoted to describing the spin dynamics of plasma electrons, being strongly disturbed by the radiative spin-flips modulated by the quasistatic plasma magnetic field (QPMF). The latter is commonly transient with a time scale as short as the driving pulse duration while being quasistatic with respect to the fast oscillating laser field. We show that the angle dependent SP of ejected electrons carries signatures of the inhomogeneous QPMF. The signal of SP of ejected electrons can be used to predict the strength of the leading order antisymmetric QPMF created by the longitudinal current. A more detailed analysis reveals that the asymmetry of SP of two outgoing divergent electron bunches characterizes the secondary QPMF, which is induced by a transverse transient current and generally neglected in previous studies [58–62]. The sum of these two part QPMFs gives rise to a nonlinear island-like magnetic structure [see Fig. 2(a)(b)]. Our results demonstrate that the spin degree of freedom of ejected electrons from ultrarelativistic plasmas can be employed in principle as a tool to retrieve information on the QPMF structure and properties.

In 2D PIC simulations, a near-critical density target is irradiated by a linearly polarized pulse (with the transverse electric field along y). Our main example adopts a peak intensity of $1.7 \times 10^{23} \text{ W/cm}^2$, equivalent to the normalized field amplitude $a_0 = 350$ given the laser wavelength $\lambda_0 = 1 \mu\text{m}$. The pulse has a $2.6 \mu\text{m}$ focal spot size and 18 fs duration (FWHM intensity measure). The target has thickness $l_0 = 10 \mu\text{m}$ and electron (carbon) density $n_e = 5n_c$ ($n_i = n_e/6$), where $n_c = m_e \omega_0^2 / 4\pi e^2$ is the plasma critical density for a laser frequency $\omega_0 = ck_0$; m_e (e) the electron mass (charge); c the speed of light. The dynamics of spin precession is governed by the Thomas-Bargmann-Michel-Telegdi equation and spin-dependent photon emissions have been implemented in the EPOCH

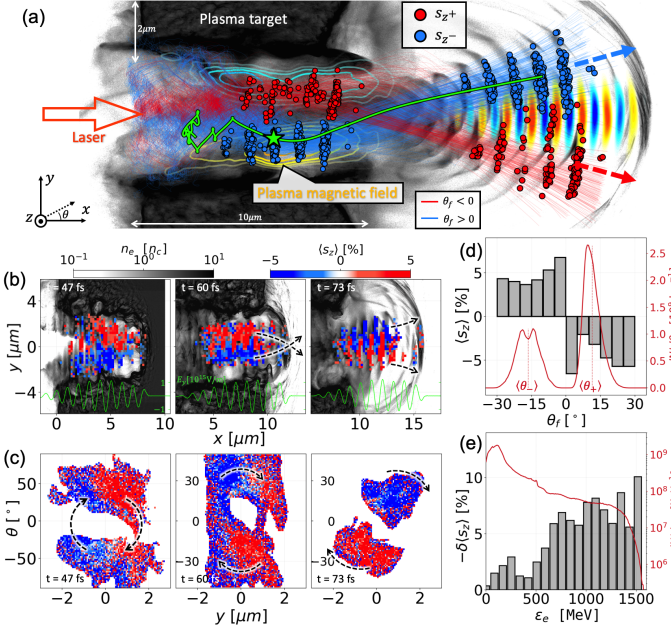


FIG. 1. (a) The interaction scheme: the laser pulse impinges on unpolarized plasma (the electron density is shown in gray shades); accelerated and radiatively polarized electrons due to spin-flips form outgoing polarized bunches. The red (blue) dots represent the electrons with spin $s_z = 1$ (-1) and the lines show their movement tendency. The green line shows a typical electron trajectory with a spin-flip marked by a pentagram. (b) and (c) show snapshots of the electron SP distribution in spatial (x, y) coordinates and transverse (y, θ) phase space, respectively. The green lines in (b) profile the laser field E_y at slice $y = 0$. (d) Angular distribution of electron number $dN/d\theta_f$ and SP $\langle s_z \rangle$. (e) $\delta \langle s_z \rangle$ and $dN/d\epsilon_e$ vs electron energy ϵ_e . All parameters are indicated in the text.

code [63], see [64].

When the pulse impinges on the target, a fraction of bulk electrons is expelled outwards by the laser ponderomotive force to form a plasma channel [65]. Meanwhile, the peripheral electrons are prone to be injected [66] and subsequently polarized inside the channel due to spin-flips during photon emissions, see Fig. 1(b). Since the ion reaction partially compensates the transverse charge separation [67], the quasistatic electric field \bar{E}_y is negligible in this scenario. Thus the deflection of the accelerated electrons in transverse direction is predominantly governed by the azimuthal QPMF \bar{B}_z , which is presumably sustained by the longitudinally forward moving electron current j_x . The simulation results in Fig. 1(a) show that the electrons with a positive (negative) final angle θ_f mainly originate from the plasma region of $y < 0$ ($y > 0$). As the magnetic field $\bar{B}_z \sim -\mu_0|j_0|y$ is antisymmetric, created by the nearly uniform current $j_x \sim -|j_0|$, the electrons exiting the plasma area with a final angle $\theta_f > 0$ mostly experience a positive \bar{B}_z [see Fig. 1(a)] and vice versa. This leads to oppositely SP ejected electron bunches: $\langle s_z \rangle < 0$ ($\langle s_z \rangle > 0$) for the electron bunch of

$\theta_f > 0$ ($\theta_f < 0$). The spatial evolution of SP in Fig. 1(b) manifests that two groups of electrons are firstly polarized and confined inside the channel, and then intersect with each other towards the opposite transverse direction. This procedure is also unveiled by the evolution of SP $\langle s_z \rangle$ in the transverse phase space (y, θ) in Fig. 1(c), where $\theta = \arctan(p_y/p_x)$ denotes the direction of electron momentum. The clockwise rotation of $\langle s_z \rangle$ indicates that the QPMF not only generates spatial dependent SP but also deflects the electrons to form an angle dependent polarization distribution of ejected electrons. In Fig. 1(d), asymmetry exists for both electron SP and number angular distributions. Specifically, the averaged SP (final angle) with a positive θ_f is $\langle s_+ \rangle \approx -3.3\%$ ($\langle \theta_+ \rangle \approx 11.4^\circ$), whereas $\langle s_- \rangle \approx 4.0\%$ ($\langle \theta_- \rangle \approx -16.5^\circ$) for $\theta_f < 0$. The magnitude of the SP signal is characterized by the parameter $\delta \langle s_z \rangle \equiv \langle s_+ \rangle - \langle s_- \rangle$. According to Fig. 1(e), SP is insignificant for low-energy electrons because of damped radiative spin-flips. Therefore, the criterion of $\epsilon_e > 4a_0 m_e c^2$ is adopted here to filter out the low-energy noise. To reveal more subtle features of QPMF \bar{B}_z , we introduce also the spin (angle) asymmetry characteristics via the absolute difference: $\Delta \langle s_z \rangle \equiv |\langle s_+ \rangle| - |\langle s_- \rangle|$ and $\Delta \langle \theta \rangle \equiv |\langle \theta_+ \rangle| - |\langle \theta_- \rangle|$, which will be discussed below.

The QPMF \bar{B}_z is determined by electric currents via $\partial \bar{B}_z / \partial y = \mu_0 j_x$ and $\partial \bar{B}_z / \partial x = -\mu_0 j_y$ (with the vacuum permeability μ_0). In general, inside a laser-driven plasma channel, the current is dominated by the longitudinal one j_x and the transverse current j_y is neglected [58–62]. However, the magnetic field in our simulation shows an irregular structure, with multiple islands associated with the current kinks and vortices, see Fig 2(b). The latter indicates that the transverse current j_y is important in characterizing the exact form of \bar{B}_z . Let us divide QPMF into two parts $\bar{B}_z = \bar{B}_{z,1} + \bar{B}_{z,2}$, where the leading part $\bar{B}_{z,1}$ is induced by j_x , while the secondary $\bar{B}_{z,2}$ by j_y : $\partial \bar{B}_{z,1} / \partial y = \mu_0 j_x$ and $\partial \bar{B}_{z,2} / \partial x = -\mu_0 j_y$. The leading part $\bar{B}_{z,1} \sim -\mu_0 |e| n_e c y$ with antisymmetric feature $\bar{B}_{z,1}(-y) = -\bar{B}_{z,1}(y)$ is ubiquitously utilized in previous studies [58–62]. Now, we focus on the secondary $\bar{B}_{z,2}$. Considering the electron velocity $v_y = p_y / (\gamma m_e c)$ and momentum $p_y \sim A_y = a_0 \cos(\xi + \phi_0)$ where $\xi = \omega_0 t - k_0 x$ and ϕ_0 the carrier envelop phase (CEP), we obtain $j_y \approx -|e| n_2 \delta(x/v_g - t) v_y dt \approx |e| n_2 \cos[\omega(x/v_g - x/v_{ph}) + \phi_0]$. The $\delta(t - x/v_g)$ function indicates that the transverse current is predominantly contributed by the electron density $n_2 \delta(t - x/v_g)$ piled up at the front edge of the plasma channel nearby the region $x \sim v_g t$, where the electron's transverse velocity is significant. Here, v_g (v_{ph}) is the laser group (phase) velocity in plasma, and the Lorentz-factor $\gamma \sim a_0$ is assumed. With $\partial \bar{B}_{z,2} / \partial x = -\mu_0 j_y$, the secondary magnetic field can be estimated:

$$\bar{B}_{z,2} \sim -\frac{\mu_0 |e| n_2}{k_2} \sin(k_2 x + \phi_0), \quad (1)$$

where $k_2 = k_0(v_{ph} - v_g)/v_g$. The analytically predicted

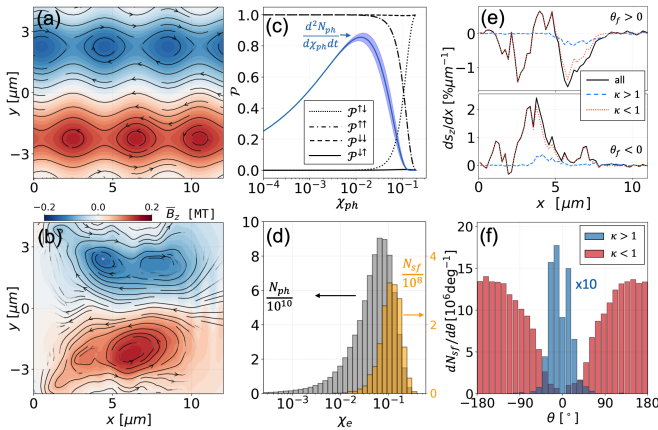


FIG. 2. The \bar{B}_z obtained from (a) analytical theory and (b) PIC simulations, where the black arrows denote the direction of electric current \mathbf{j} . (c) Probabilities \mathcal{P} of electron spin-flip after emitting a photon with χ_{ph} . The $\uparrow\downarrow$ represents the spin-flip from parallel to antiparallel with respect to the magnetic field direction. The blue line profiles the photon emission probability $d^2N_{ph}/d\chi_{ph}dt$ with a bandwidth accounting for the influence of electron spin. (d) The number distribution of all emitted photons N_{ph} (grey) and emission associated with spin-flips N_{sf} (yellow). (e) The spatial dependent SP differentiate ds_z/dx contributed by the cases of $\kappa \leq 1$ for electrons with final angle $\theta_f > 0$ and $\theta_f < 0$, respectively. (f) The angular dependence of spin-flip occurrence, where the result of condition $\kappa > 1$ is multiplied by 10 for better visibility.

$\bar{B}_z = \bar{B}_{z,1} + \bar{B}_{z,2}$ is shown in Fig. 2(a), which agrees qualitatively with the simulated \bar{B}_z in Fig. 2(b). The asymmetric periodic island-like structure of QPMF \bar{B}_z stems from the nontrivial current vortex $(\nabla \times \mathbf{j})_{x,y} \neq 0$ generated by the transverse current of electrons plough away by the laser beam front.

As we are interested in the relation of the electron SP to the magnetic field structure, and considering the polarization attributable to the spin-flip during a photon emission, we analyze the probability of this process $\mathcal{P}(\chi_{ph})$ in Fig. 2(c) for typical parameters of our PIC simulations. Here, the electron with an initial $\gamma_e = 2000$ normally crosses the uniform magnetic field $B_0 = 10^4$ T, and the electron quantum invariant parameter is $\chi_e \sim 0.1$, with $\chi_{e,ph} \equiv (e\hbar/m_e^3c^4)|F_{\mu\nu}p^\nu|$ and the momentum p^ν of the electron or photon, respectively. As Fig. 2(c) illustrates, the electron spin-flips exclusively take place when emitting an energetic photon with χ_{ph} close to χ_e , while the photon emission probability is peaked at $\hbar\omega_c \sim \chi_e\gamma_e m_e c^2$ (at $\chi_e < 1$), i.e., the peak of the spin-flip process is shifted with respect to the photon emission to higher χ_e 's, see Fig. 2(d). Both the laser magnetic field B_l and QPMF \bar{B}_z can cause the electron spin-flip as $\chi_e \approx \gamma_e/[(1 - \cos\theta)B_l + \bar{B}_z]/B_c$ with the Schwinger limit $B_c \approx 4 \times 10^9$ T. We introduce the parameter $\kappa = |\bar{B}_z/[(1 - \cos\theta)B_l]|$, defining two regimes, when the electron spin-flip is dominated by the plasma

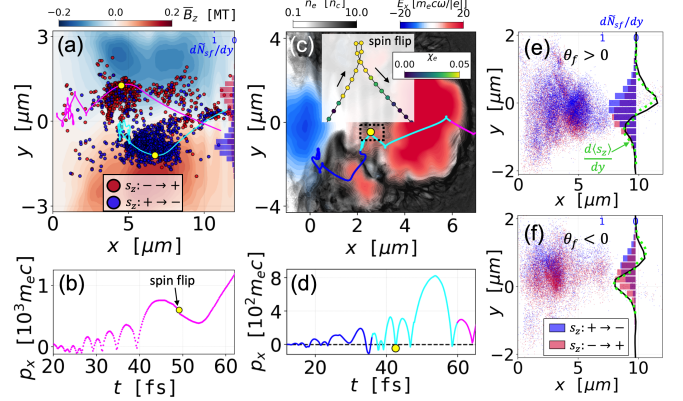


FIG. 3. (a) The red (blue) dots present the electron spin-flip from $s_z = -1$ (1) to 1 (-1) in the plasma field dominant regime ($\kappa > 1$) and the histogram exhibits its dependence on the transverse coordinate $d\bar{N}_{sf}/dy$. The magenta line refers to a typical electron trajectory and its time evolution of p_x is in (b). (c) The typical electron trajectory for the regime $\kappa < 1$ and its corresponding momentum evolution in (d). The spin-flips of electron trajectories in (a)-(d) are marked by yellow circles. (e) and (f) show the spin-flips with $\kappa < 1$ for electrons with final angle $\theta_f > 0$ and $\theta_f < 0$, where the solid black (dashed lime) lines profile the simulated (analytically derived) dependence of net electron SP s_z on the coordinate y .

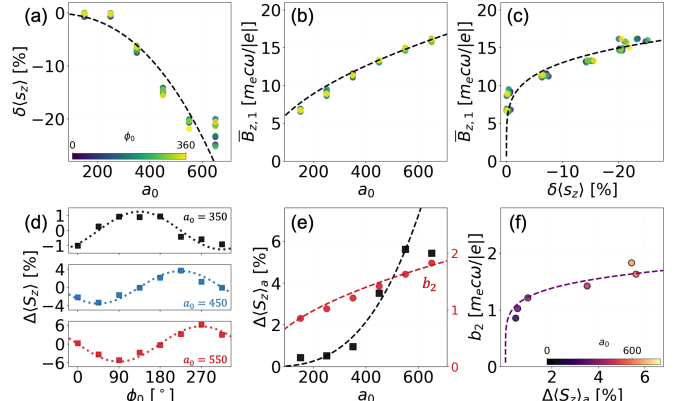


FIG. 4. The dependence of (a) electron SP $\delta \langle s_z \rangle$ and (b) the leading order QPMF $\bar{B}_{z,1}$ on a_0 . (c) The correlation between $\delta \langle s_z \rangle$ and $\bar{B}_{z,1}$. In (a)-(c), the dots refer to the simulation results with different laser CEP ϕ_0 while the dashed black line denotes the theory. (d) The dependence of $\Delta \langle s_z \rangle$ on ϕ_0 for different a_0 . (e) The dependence of $\Delta \langle s_z \rangle_a$ and b_2 on a_0 . (f) The correlation between the amplitude of the SP asymmetry $\Delta \langle s_z \rangle_a$ and the secondary QPMF b_2 .

($\kappa > 1$) or by the laser field ($\kappa < 1$). The evolution of SP in Fig. 2(e) demonstrates that the laser field dominated regime ($\kappa < 1$) mostly contributes to the final electron SP. A distinguishable feature between the $\kappa \leq 1$ regimes is the angle θ of the electron's instantaneous momentum when the spin-flip occurs. As the angular dependent spin-flip shows in Fig. 2(f), the $\kappa < 1$ regime applies at backward emissions, while $\kappa > 1$ for forward ones.

The detailed particle tracking further confirms these conclusions. In the $\kappa > 1$ regime Figs. 3(a),(b), the position of spin-flip with $\kappa > 1$ is closely correlated with the spatial distribution of QPMF \bar{B}_z . The time evolution of p_x illustrates that the spin-flip happens after the electron starts an efficient acceleration and its velocity aligns longitudinally $\theta \ll 1$, resulting in $(1 - \cos \theta)B_l < \bar{B}_z$. For the laser dominant regime $\kappa < 1$, the electron trajectory and momentum evolution [in Fig. 3(c)(d)] demonstrate that the typical spin-flip occurs at the electron's temporarily backward motion, when $(1 - \cos \theta) \sim 1$ and $B_l > \bar{B}_z$.

It should be noted that even in the laser dominant regime, the QPMF \bar{B}_z is still the key factor for the SP. The reason is that the laser field has oscillating character. Although it can cause spin-flips, its net contribution to the final SP is negligible. The laser magnetic field B_l acts as a catalyst to enhance the electron spin-flips by increasing χ_e and net spin-flips contributing to the final SP are still determined by \bar{B}_z [64]. We may estimate $s_z \approx -\int \bar{B}_z / |B_l| \mathcal{A}(\chi_e) dt$ (at $B_l \gg \bar{B}_z$), with $\mathcal{A}(\chi_e) = (\sqrt{3}\alpha_f m_e c^2 \chi_e) / (h\gamma_e) \mathcal{A}^*(\chi_e)$, and $\mathcal{A}^*(\chi_e) \approx 0.18\chi_e$ (at $0.01 < \chi_e < 0.4$) [64]. The electrons with final angle $\theta_f > 0$ ($\theta_f < 0$) are mainly exposed to the QPMF $\bar{B}_z > 0$ ($\bar{B}_z < 0$) at the region $y < 0$ ($y > 0$), and the overall SP with $\theta_f > 0$ ($\theta_f < 0$) would be $s_z < 0$ ($s_z > 0$) which are illustrated as the solid black lines in Fig. 3(e)(f).

Thus, we calculate the electron's SP magnitude $\delta \langle s_z \rangle$ being correlated with the leading order QPMF $\bar{B}_{z,1}$:

$$\delta \langle s_z \rangle \sim -\eta \frac{|e||\bar{B}_{z,1}|}{m_e \omega_0} a_0^2, \quad (2)$$

where $\gamma_e \sim a_0$ is used, and $\eta \approx 4 \times 10^{-8}$ accounts for the deviations from the radiative spin evolution. With $\bar{B}_{z,1} \approx \sqrt{(a_0/4\pi)(n_e/n_c)}(m_e \omega_0/|e|)$, we find the SP scaling $\delta \langle s_z \rangle \propto a_0^{5/2}$, as well as the relation $\bar{B}_{z,1} \approx [-(\delta \langle s_z \rangle / \eta)(n_e/4\pi n_c)^2]^{1/5}$. In Fig. 4(a)(b),(c), the analytically predicted scalings of $\delta \langle s_z \rangle$ and $\bar{B}_{z,1}$ are in good accordance with the 2D simulation results.

Finally, we show how with the help of the SP asymmetry signal $\Delta \langle s_z \rangle$ defined above, the secondary QPMF can be retrieved. In the $\Delta \langle s_z \rangle$ signal the contribution of the $\bar{B}_{z,1}$ is cancelled, and $\Delta \langle s_z \rangle \approx 2 \int (\bar{B}_{z,2} / |B_l|) \mathcal{A}(\chi_e) dt$. Since $\bar{B}_{z,2} \sim b_2 \sin(k_2 x + \phi_0)$ is oscillating along the longitudinal position (along the laser CEP), the overall effect of $\bar{B}_{z,2}$ imprinted on the signal of $\Delta \langle s_z \rangle$ is oscillating as well. Taking into account the results for $\delta \langle s_z \rangle$ and $\bar{B}_{z,2}$, we find for the asymmetry signal

$$\Delta \langle s_z \rangle \sim \delta \langle s_z \rangle \frac{b_2}{|\bar{B}_{z,1}|} \frac{k_0}{k_2} \cos(k_2 l_0 + \phi_0), \quad (3)$$

where b_2 is the amplitude of $\bar{B}_{z,2}$. The oscillating dependence of $\Delta \langle s_z \rangle$ on the laser CEP ϕ_0 is reproduced by the simulation results in Fig. 4(d). We see that the amplitude of the SP asymmetry signal $\Delta \langle s_z \rangle_a$ is directly related to the secondary QPMF b_2 :

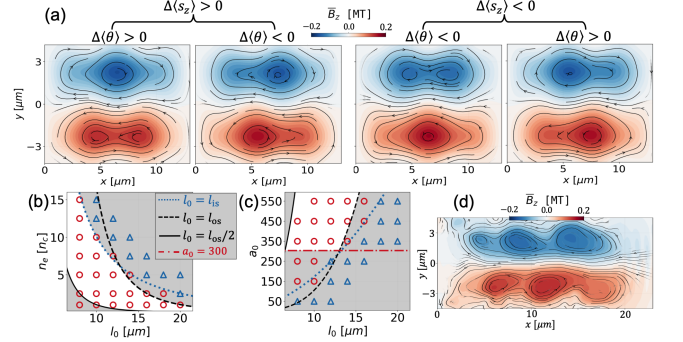


FIG. 5. (a) The \bar{B}_z predicted by the model based on the sign of $\Delta \langle s_z \rangle$ and $\Delta \langle \theta \rangle$. The valid range of the model is illustrated in the white region of the parameter space in (b) $a_0 = 350$ and (c) $n_e = 5n_c$, where the circles (triangles) mark the simulation results of \bar{B}_z with no more (more) than two islands on each side of $y = 0$. (d) The \bar{B}_z obtained from simulation for the case of $a_0 = 350$, $n_e = 5n_c$, and $l_0 = 20\mu\text{m}$.

$\Delta \langle s_z \rangle_a \sim |\delta \langle s_z \rangle| (b_2 / |\bar{B}_{z,1}|) (k_0 / k_2) \sim \eta \sqrt{n_c / n_e} b_2 a_0^{5/2}$ [see Fig. 4(e)], where $k_0 / k_2 \sim (a_0 n_c / n_e)^{1/2}$ is obtained from simulation results [64]. Moreover, the amplitude of the secondary quasistatic magnetic field $b_2 \approx 0.03 \sqrt{a_0 (n_e / n_c)} (m_e \omega_0 / |e|)$ can be estimated through the number conservation between the initial undisturbed plasma and the electrons piled up at the front of the channel edge. Then, the correlation between $\Delta \langle s_z \rangle_a$ and b_2 is established: $b_2 \sim 0.12 [\Delta \langle s_z \rangle_a / \eta]^{1/6}$, which is in reasonable agreement with the simulation results [see Fig. 4(f)]. Therefore, the SP signals of $\delta \langle s_z \rangle$ and $\Delta \langle s_z \rangle$ allow to retrieve the strength of the leading and secondary QPMFs.

In addition, the combination of $\Delta \langle s_z \rangle$ and $\Delta \langle \theta \rangle$, allows to predict the concrete spatial structure of \bar{B}_z , see Fig. 5(a). Based on the sign of $\Delta \langle s_z \rangle$ and $\Delta \langle \theta \rangle$, the analytically estimated magnetic island structures agree well with the simulation results, see [64]. We define the limitations of the presented field retrieval model. Firstly, it is applicable when no more than two QPMF islands exist at $y \leq 0$, with a criterion $l_0 < l_{\text{island}} \sim 1.7\lambda_0(a_0 n_c / n_e)^{1/2}$ [64]. Secondly, to exclude the influence of depolarization, the ejected electrons should experience a half-period of betatron oscillation inside the channel, with a criterion $0.5l_{\text{os}} < l_0 < l_{\text{os}} \sim 5\lambda_0(a_0 n_c / n_e)^{1/4}$ [64]. Consequently, the valid range of the model is $0.5l_{\text{os}} < l_0 < \min\{l_{\text{is}}, l_{\text{os}}\}$ shown as the white area in Fig. 5(b)(c). Our method based on the electron radiative polarization will be efficient in the quantum radiation dominated regime at $\alpha_f a_0 \chi_e \gtrsim 1$ (approximately at $a_0 \gtrsim 300$) and $\chi_e \gtrsim 0.1$ [26], with a SP signal within the precision of the electron polarimetry of $\sim 0.4\%$ [68]. The requirement might be relieved at alternative setups [29], e.g., in multiple colliding laser pulses [69], where new schemes for the magnetic field retrieval may be needed.

To confirm the robustness of our scheme, we also inves-

tigated the role of experimental imperfections and uncertainties, in particular, the asymmetry in the driving laser pulse, and the ramp-up and -down of the plasma density profile [64]. The simulation results indicate that the presented scheme is robust to moderate imperfections of such practical issues. It should be noted that distinguishing more complex field structures, e.g., the three-island structure like that in Fig. 5(d), could be achievable with modifications of the retrieval method, see an example in [64], which however needs further exploration.

In conclusion, the ejected electron spin provides a new degree of freedom to extract information on the structure and magnitude of different components of the transient plasma fields. Our results open a new avenue for the electron spin-based plasma diagnostics in extreme conditions, which are prevalent in astrophysical environments and are expected in near future laser facilities.

The original version of code EPOCH adapted here is funded by the UK EPSRC grants EP/G054950/1, EP/G056803/1, EP/G055165/1 and EP/M022463/1. Z. Gong would like to thank A. V. Arefiev, X.-Q. Yan and J.-X. Li for useful discussions. The Supplemental Material includes Refs. [70–78].

* gong@mpi-hd.mpg.de

† k.hatsagortsyan@mpi-hd.mpg.de

- [1] D. Lai, Matter in strong magnetic fields, *Reviews of Modern Physics* **73**, 629 (2001).
- [2] T. Piran, The physics of gamma-ray bursts, *Reviews of Modern Physics* **76**, 1143 (2005).
- [3] R. Ruffini, G. Vereshchagin, and S.-S. Xue, Electron-positron pairs in physics and astrophysics: from heavy nuclei to black holes, *Physics Reports* **487**, 1 (2010).
- [4] A. Bohdan, M. Pohl, J. Niemiec, P. J. Morris, Y. Matsumoto, T. Amano, M. Hoshino, and A. Sulaiman, Magnetic field amplification by the weibel instability at planetary and astrophysical shocks with high mach number, *Phys. Rev. Lett.* **126**, 095101 (2021).
- [5] A. Philippov, A. Timokhin, and A. Spitkovsky, Origin of pulsar radio emission, *Phys. Rev. Lett.* **124**, 245101 (2020).
- [6] K. Jedamzik and L. Pogosian, Relieving the hubble tension with primordial magnetic fields, *Phys. Rev. Lett.* **125**, 181302 (2020).
- [7] J. W. Foster, Y. Kahn, O. Macias, Z. Sun, R. P. Eatough, V. I. Kondratiev, W. M. Peters, C. Weniger, and B. R. Safdi, Green bank and effelsberg radio telescope searches for axion dark matter conversion in neutron star magnetospheres, *Phys. Rev. Lett.* **125**, 171301 (2020).
- [8] M. Tatarakis, I. Watts, F. Beg, E. Clark, A. Dangor, A. Gopal, M. Haines, P. Norreys, U. Wagner, M.-S. Wei, et al., Measuring huge magnetic fields, *Nature* **415**, 280 (2002).
- [9] G. Sarri, A. Macchi, C. A. Cecchetti, S. Kar, T. V. Liseykina, X. H. Yang, M. E. Dieckmann, J. Fuchs, M. Galimberti, L. A. Gizzi, R. Jung, I. Kourakis, J. Osterholz, F. Pegoraro, A. P. L. Robinson, L. Romagnani, O. Willi, and M. Borghesi, Dynamics of self-generated, large amplitude magnetic fields following high-intensity laser matter interaction, *Phys. Rev. Lett.* **109**, 205002 (2012).
- [10] W. Schumaker, N. Nakanii, C. McGuffey, C. Zulick, V. Chyvkov, F. Dollar, H. Habara, G. Kalintchenko, A. Maksimchuk, K. A. Tanaka, A. G. R. Thomas, V. Yanovsky, and K. Krushelnick, Ultrafast electron radiography of magnetic fields in high-intensity laser-solid interactions, *Phys. Rev. Lett.* **110**, 015003 (2013).
- [11] J. Meinecke, H. Doyle, F. Miniati, A. R. Bell, R. Birmingham, R. Crowston, R. Drake, M. Fatenejad, M. Koenig, Y. Kuramitsu, et al., Turbulent amplification of magnetic fields in laboratory laser-produced shock waves, *Nature Physics* **10**, 520 (2014).
- [12] C. Huntington, F. Fiua, J. Ross, A. Zylstra, R. Drake, D. Froula, G. Gregori, N. Kugland, C. Kuranz, M. Levy, et al., Observation of magnetic field generation via the weibel instability in interpenetrating plasma flows, *Nature Physics* **11**, 173 (2015).
- [13] B. Albertazzi, A. Ciardi, M. Nakatsutsumi, T. Vinci, J. Béard, R. Bonito, J. Billette, M. Borghesi, Z. Burkley, S. Chen, et al., Laboratory formation of a scaled protostellar jet by coaligned poloidal magnetic field, *Science* **346**, 325 (2014).
- [14] G. Revet, S. N. Chen, R. Bonito, B. Khiar, E. Filippov, C. Argiroff, D. P. Higginson, S. Orlando, J. Béard, M. Blecher, et al., Laboratory unraveling of matter accretion in young stars, *Science advances* **3**, e1700982 (2017).
- [15] G. Revet, B. Khiar, E. Filippov, C. Argiroff, J. Béard, R. Bonito, M. Cerchez, S. Chen, T. Gangolf, D. Higginson, et al., Laboratory disruption of scaled astrophysical outflows by a misaligned magnetic field, *Nature communications* **12**, 1 (2021).
- [16] The Vulcan facility, <https://www.clf.stfc.ac.uk/Pages/The-Vulcan-10-Petawatt-Project.aspx>.
- [17] The Extreme Light Infrastructure (ELI), <http://www.eli-laser.eu/>.
- [18] ELI-Beamlines, <https://www.eli-beams.eu/en/facility/lasers/>.
- [19] Exawatt Center for Extreme Light Studies (XCELS), <http://www.xcels.iapras.ru/>.
- [20] C. N. Danson, C. Haefner, J. Bromage, T. Butcher, J.-C. F. Chanteloup, E. A. Chowdhury, A. Galvanauskas, L. A. Gizzi, J. Hein, D. I. Hillier, et al., Petawatt and exawatt class lasers worldwide, *High Power Laser Science and Engineering* **7** (2019).
- [21] J. W. Yoon, C. Jeon, J. Shin, S. K. Lee, H. W. Lee, I. W. Choi, H. T. Kim, J. H. Sung, and C. H. Nam, Achieving the laser intensity of $5.5 \times 10^{22} \text{ W/cm}^2$ with a wavefront-corrected multi-pw laser, *Optics express* **27**, 20412 (2019).
- [22] J. W. Yoon, Y. G. Kim, I. W. Choi, J. H. Sung, H. W. Lee, S. K. Lee, and C. H. Nam, Realization of laser intensity over 10^{23} W/cm^2 , *Optica* **8**, 630 (2021).
- [23] G. A. Mourou, T. Tajima, and S. V. Bulanov, Optics in the relativistic regime, *Reviews of modern physics* **78**, 309 (2006).
- [24] M. Marklund and P. K. Shukla, Nonlinear collective effects in photon-photon and photon-plasma interactions, *Reviews of modern physics* **78**, 591 (2006).
- [25] A. Bell and J. G. Kirk, Possibility of prolific pair production with high-power lasers, *Physical review letters* **101**, 200403 (2008).

[26] A. Di Piazza, C. Müller, K. Hatsagortsyan, and C. H. Keitel, Extremely high-intensity laser interactions with fundamental quantum systems, *Reviews of Modern Physics* **84**, 1177 (2012).

[27] S. Bulanov, T. Z. Esirkepov, M. Kando, J. Koga, K. Kondo, and G. Korn, On the problems of relativistic laboratory astrophysics and fundamental physics with super powerful lasers, *Plasma Physics Reports* **41**, 1 (2015).

[28] K. Poder, M. Tamburini, G. Sarri, A. Di Piazza, S. Kuschel, C. Baird, K. Behm, S. Bohlen, J. Cole, D. Corvan, et al., Experimental signatures of the quantum nature of radiation reaction in the field of an ultraintense laser, *Physical Review X* **8**, 031004 (2018).

[29] J. Cole, K. Behm, E. Gerstmayr, T. Blackburn, J. Wood, C. Baird, M. J. Duff, C. Harvey, A. Ilderton, A. Joglekar, et al., Experimental evidence of radiation reaction in the collision of a high-intensity laser pulse with a laser-wakefield accelerated electron beam, *Physical Review X* **8**, 011020 (2018).

[30] C. Li, F. Séguin, J. Frenje, J. Rygg, R. Petrasso, R. Town, P. Amendt, S. Hatchett, O. Landen, A. Mackinnon, et al., Observation of the decay dynamics and instabilities of megagauss field structures in laser-produced plasmas, *Physical review letters* **99**, 015001 (2007).

[31] L. Willingale, A. Thomas, P. Nilson, M. Kaluza, S. Bandyopadhyay, A. Dangor, R. Evans, P. Fernandes, M. Haines, C. Kamperidis, et al., Fast advection of magnetic fields by hot electrons, *Physical review letters* **105**, 095001 (2010).

[32] A. Macchi, M. Borghesi, and M. Passoni, Ion acceleration by superintense laser-plasma interaction, *Reviews of Modern Physics* **85**, 751 (2013).

[33] L. Lancia, B. Albertazzi, C. Boniface, A. Grisollet, R. Riquier, F. Chaland, K.-C. Le Thanh, P. Mellor, P. Antici, S. Buffeuchoux, et al., Topology of megagauss magnetic fields and of heat-carrying electrons produced in a high-power laser-solid interaction, *Physical review letters* **113**, 235001 (2014).

[34] C. Zhang, J. Hua, Y. Wu, Y. Fang, Y. Ma, T. Zhang, S. Liu, B. Peng, Y. He, C.-K. Huang, et al., Measurements of the growth and saturation of electron weibel instability in optical-field ionized plasmas, *Physical Review Letters* **125**, 255001 (2020).

[35] A. F. Bott, P. Tzeferacos, L. Chen, C. A. Palmer, A. Rigby, A. R. Bell, R. Bingham, A. Birkel, C. Graziani, D. H. Froula, et al., Time-resolved turbulent dynamo in a laser plasma, *Proceedings of the National Academy of Sciences* **118** (2021).

[36] M. Tatarakis, A. Gopal, I. Watts, F. Beg, A. Dangor, K. Krushelnick, U. Wagner, P. Norreys, E. Clark, M. Zepf, et al., Measurements of ultrastrong magnetic fields during relativistic laser-plasma interactions, *Physics of Plasmas* **9**, 2244 (2002).

[37] M. Kaluza, H.-P. Schlenvoigt, S. Mangles, A. Thomas, A. Dangor, H. Schwoerer, W. Mori, Z. Najmudin, and K. Krushelnick, Measurement of magnetic-field structures in a laser-wakefield accelerator, *Physical review letters* **105**, 115002 (2010).

[38] A. Buck, M. Nicolai, K. Schmid, C. M. Sears, A. Sävert, J. M. Mikhailova, F. Krausz, M. C. Kaluza, and L. Veisz, Real-time observation of laser-driven electron acceleration, *Nature Physics* **7**, 543 (2011).

[39] S. Zhou, Y. Bai, Y. Tian, H. Sun, L. Cao, and J. Liu, Self-organized kilotesla magnetic-tube array in an expand-

ing spherical plasma irradiated by khz femtosecond laser pulses, *Physical review letters* **121**, 255002 (2018).

[40] T. Wang, T. Toncian, M. Wei, and A. Arefiev, Structured targets for detection of megatesla-level magnetic fields through faraday rotation of xfel beams, *Physics of plasmas* **26**, 013105 (2019).

[41] T. Jungwirth, J. Wunderlich, V. Novák, K. Olejník, B. Gallagher, R. Campion, K. Edmonds, A. Rushforth, A. Ferguson, and P. Němec, Spin-dependent phenomena and device concepts explored in (ga, mn) as, *Reviews of Modern Physics* **86**, 855 (2014).

[42] K. Abe, T. Akagi, P. Anthony, R. Antonov, R. Arnold, T. Averett, H. Band, J. Bauer, H. Borel, P. Bosted, et al., Precision measurement of the deuteron spin structure function g 1 d, *Phys. Rev. Lett.* **75**, 25 (1995).

[43] G. Moortgat-Pick, T. Abe, G. Alexander, B. Ananthanarayan, A. Babich, V. Bharadwaj, D. Barber, A. Bartl, A. Brachmann, S. Chen, et al., Polarized positrons and electrons at the linear collider, *Physics Reports* **460**, 131 (2008).

[44] M. W. Walser, D. J. Urbach, K. Z. Hatsagortsyan, S. X. Hu, and C. H. Keitel, Spin and radiation in intense laser fields, *Phys. Rev. A* **65**, 043410 (2002).

[45] D. Del Sorbo, D. Seipt, T. G. Blackburn, A. G. R. Thomas, C. D. Murphy, J. G. Kirk, and C. P. Ridgers, Spin polarization of electrons by ultraintense lasers, *Phys. Rev. A* **96**, 043407 (2017).

[46] D. Seipt, D. Del Sorbo, C. P. Ridgers, and A. G. R. Thomas, Theory of radiative electron polarization in strong laser fields, *Phys. Rev. A* **98**, 023417 (2018).

[47] D. D. Sorbo, D. Seipt, A. G. R. Thomas, and C. P. Ridgers, Electron spin polarization in realistic trajectories around the magnetic node of two counter-propagating, circularly polarized, ultra-intense lasers, *Plasma Phys. Control. Fusion* **60**, 064003 (2018).

[48] Y.-F. Li, Y.-Y. Chen, W.-M. Wang, and H.-S. Hu, Production of highly polarized positron beams via helicity transfer from polarized electrons in a strong laser field, *Physical Review Letters* **125**, 044802 (2020).

[49] A. A. Sokolov and I. M. Ternov, *Synchrotron Radiation* (Akademie, Germany, 1968).

[50] V. N. Baier and V. M. Katkov, Radiational polarization of electrons in inhomogeneous magnetic field, *Phys. Lett. A* **24**, 327 (1967).

[51] V. N. Baier, Radiative polarization of electron in storage rings, *Sov. Phys. Usp.* **14**, 695 (1972).

[52] Y. Derbenev and A. M. Kondratenko, Polarization kinematics of particles in storage rings, *Sov. Phys. JETP* **37**, 968 (1973).

[53] Y.-F. Li, R. Shaisultanov, K. Z. Hatsagortsyan, F. Wan, C. H. Keitel, and J.-X. Li, Ultrarelativistic electron-beam polarization in single-shot interaction with an ultraintense laser pulse, *Physical review letters* **122**, 154801 (2019).

[54] Y.-F. Li, R.-T. Guo, R. Shaisultanov, K. Z. Hatsagortsyan, and J.-X. Li, Electron polarimetry with nonlinear compton scattering, *Physical Review Applied* **12**, 014047 (2019).

[55] F. Wan, R. Shaisultanov, Y.-F. Li, K. Z. Hatsagortsyan, C. H. Keitel, and J.-X. Li, Ultrarelativistic polarized positron jets via collision of electron and ultraintense laser beams, *Phys. Lett. B* **800**, 135120 (2020).

[56] Y.-Y. Chen, P.-L. He, R. Shaisultanov, K. Z. Hatsagortsyan, and C. H. Keitel, Polarized positron beams via in-

tense two-color laser pulses, *Physical review letters* **123**, 174801 (2019).

[57] D. Seipt, D. Del Sorbo, C. P. Ridgers, and A. G. R. Thomas, Ultrafast polarization of an electron beam in an intense bichromatic laser field, *Phys. Rev. A* **100**, 061402(R) (2019).

[58] A. Pukhov and J. Meyer-ter Vehn, Relativistic magnetic self-channeling of light in near-critical plasma: three-dimensional particle-in-cell simulation, *Physical review letters* **76**, 3975 (1996).

[59] A. Pukhov, Z.-M. Sheng, and J. Meyer-ter Vehn, Particle acceleration in relativistic laser channels, *Physics of Plasmas* **6**, 2847 (1999).

[60] D. Stark, T. Toncian, and A. Arefiev, Enhanced multi-mev photon emission by a laser-driven electron beam in a self-generated magnetic field, *Physical review letters* **116**, 185003 (2016).

[61] Z. Gong, F. Mackenroth, T. Wang, X. Yan, T. Toncian, and A. Arefiev, Direct laser acceleration of electrons assisted by strong laser-driven azimuthal plasma magnetic fields, *Physical Review E* **102**, 013206 (2020).

[62] A. E. Hussein, A. V. Arefiev, T. Batson, H. Chen, R. Craxton, *et al.*, Towards the optimisation of direct laser acceleration, *New Journal of Physics* **23**, 023031 (2021).

[63] T. Arber, K. Bennett, C. Brady, A. Lawrence-Douglas, M. Ramsay, N. Sircombe, P. Gillies, R. Evans, H. Schmitz, A. Bell, *et al.*, Contemporary particle-in-cell approach to laser-plasma modelling, *Plasma Physics and Controlled Fusion* **57**, 113001 (2015).

[64] See the Supplemental Materials for the details.

[65] A. Pukhov, Strong field interaction of laser radiation, *Reports on progress in Physics* **66**, 47 (2002).

[66] L. Ji, A. Pukhov, I. Y. Kostyukov, B. Shen, and K. Akli, Radiation-reaction trapping of electrons in extreme laser fields, *Physical review letters* **112**, 145003 (2014).

[67] O. Jansen, T. Wang, D. J. Stark, E. d'Humières, T. Toncian, and A. Arefiev, Leveraging extreme laser-driven magnetic fields for gamma-ray generation and pair production, *Plasma Physics and Controlled Fusion* **60**, 054006 (2018).

[68] A. Narayan, D. Jones, J. Cornejo, M. Dalton, W. Deconinck, D. Dutta, D. Gaskell, J. Martin, K. Paschke, V. Tsvaskis, *et al.*, Precision electron-beam polarimetry at 1 gev using diamond microstrip detectors, *Physical Review X* **6**, 011013 (2016).

[69] P. Zhang, S. Bulanov, D. Seipt, A. Arefiev, and A. Thomas, Relativistic plasma physics in supercritical fields, *Physics of Plasmas* **27**, 050601 (2020).

[70] L. H. Thomas, I. the kinematics of an electron with an axis, *The London, Edinburgh, and Dublin Philosophical Magazine and Journal of Science* **3**, 1 (1927).

[71] V. Bargmann, L. Michel, and V. Telegdi, Precession of the polarization of particles moving in a homogeneous electromagnetic field, *Physical Review Letters* **2**, 435 (1959).

[72] R. Duclous, J. G. Kirk, and A. R. Bell, Monte carlo calculations of pair production in high-intensity laser-plasma interactions, *Plasma Physics and Controlled Fusion* **53**, 015009 (2010).

[73] N. Elkina, A. Fedotov, I. Y. Kostyukov, M. Legkov, N. Narozhny, E. Nerush, and H. Ruhl, Qed cascades induced by circularly polarized laser fields, *Physical Review Special Topics-Accelerators and Beams* **14**, 054401 (2011).

[74] C. Ridgers, J. G. Kirk, R. Duclous, T. Blackburn, C. Brady, K. Bennett, T. Arber, and A. Bell, Modelling gamma-ray photon emission and pair production in high-intensity laser-matter interactions, *Journal of Computational Physics* **260**, 273 (2014).

[75] A. Gonoskov, S. Bastrakov, E. Efimenko, A. Ilderton, M. Marklund, I. Meyerov, A. Muraviev, A. Sergeev, I. Surmin, and E. Wallin, Extended particle-in-cell schemes for physics in ultrastrong laser fields: Review and developments, *Physical Review E* **92**, 023305 (2015).

[76] W. Ma, L. Song, R. Yang, T. Zhang, Y. Zhao, L. Sun, Y. Ren, D. Liu, L. Liu, J. Shen, *et al.*, Directly synthesized strong, highly conducting, transparent single-walled carbon nanotube films, *Nano Letters* **7**, 2307 (2007).

[77] J. Bin, W. Ma, H. Wang, M. Streeter, C. Kreuzer, D. Kiefer, M. Yeung, S. Cousens, P. Foster, B. Dromey, *et al.*, Ion acceleration using relativistic pulse shaping in near-critical-density plasmas, *Physical review letters* **115**, 064801 (2015).

[78] H. Wang, C. Lin, Z. Sheng, B. Liu, S. Zhao, Z. Guo, Y. Lu, X. He, J. Chen, and X. Yan, Laser shaping of a relativistic intense, short gaussian pulse by a plasma lens, *Physical review letters* **107**, 265002 (2011).